JOURNAL OF THERMOPHYSICS AND HEAT TRANSFER
Vol. 19, No. 3, July–September 2005

Estimation of Microwave Radiation Intensity from a Multilayered Cloud Model

V. Swaminathan*
Indian Institute of Technology Madras, Chennai 600 036, India
R. M. Gairola†
Space Applications Centre, Ahmedabad 380 015, India
and
C. Balaji‡ and S. P. Venkateshan§
Indian Institute of Technology Madras, Chennai 600 036, India

A direct analysis for the estimation of brightness temperatures in realistic, multilayered cloud hydrometeor profiles over a range of microwave frequencies (6.6–183 GHz) is presented. The sensitivity of microwave radiative transfer through the atmosphere with respect to its constituents is investigated with a one-dimensional numerical model. The atmosphere is modeled as nongray, absorbing, emitting, and anisotropically scattering with nonisothermal, vertically stratified layers. The governing time-independent radiative heat transfer equation through the atmosphere is solved using a finite volume method. Results of homogeneous and inhomogeneous media, in the presence and absence of scattering constituents, are compared to those published earlier. In the absence of scattering constituents, the differences in the brightness temperature values between the present study and with those published earlier never exceeded 2 K, and the differences that are caused in the presence of scattering constituents are discussed.

Nomenclature

A	=	area, m^2
C_1	=	first radiation constant, 0.59552197×10^8 $W\mu m^4/(m^2 sr)$
C_2	=	second radiation constant, 14387.69 μmK
g	=	asymmetry factor
I	=	radiation intensity, $Wm^{-2}sr^{-1}$
$\bar{I}$	=	in-scattering term, $Wm^{-2}sr^{-1}$
$\hat{\boldsymbol{i}}, \hat{\boldsymbol{j}}, \hat{\boldsymbol{k}}$	=	unit vectors along x, y, and z coordinate directions
M	=	number of directions in γ direction
N	=	number of control volumes
n	=	number of layers
$\boldsymbol{n}$	=	unit vector normal to a control volume surface
q	=	total heat transfer rate per unit width from the hot wall, Wm^{-1}
q^*	=	dimensionless heat flux
R	=	$(\kappa I_b + \sigma_s \bar{I})/\beta$, $Wm^{-2}sr^{-1}$
S	=	distance between interpolation point uf and integration point f, m
s	=	coordinate along ray path, m
$\boldsymbol{s}$	=	unit direction vector
T	=	absolute temperature, K
v	=	elemental volume, m^3
z	=	coordinate along vertical direction, m
β	=	extinction coefficient, m^{-1}
γ	=	polar angle, rad
Δz	=	thickness of control volume, m
ε	=	emissivity of surface
κ	=	absorption coefficient, m^{-1}
λ	=	wavelength, μm
σ	=	Stefan–Boltzmann constant, 5.67×10^{-8} $Wm^{-2}K^{-4}$
σ_s	=	scattering coefficient, m^{-1}
Φ	=	phase function for scattering
ϕ	=	azimuthal angle, rad
ω	=	solid angle, sr

Subscripts

b	=	blackbody
bs	=	bottom surface or bottom plate
f	=	integration point
n, s	=	north and south faces of the control volume
P, N, S	=	nodes within control volumes
uf	=	interpolation point
us	=	upper surface or upper plate
z	=	z direction
λ	=	spectral quantity

Superscripts

ℓ	=	corresponding to direction
,	=	incoming direction

Introduction

THE interaction of thermal radiation with an absorbing, emitting, and scattering (radiatively participating) medium continues to draw significant attention, prompted by numerous engineering applications. Examples are many, notably in combustion chambers, nuclear explosions, and atmospheric and space applications. Satellite-based techniques for measuring precipitation in the atmosphere exists for visible, infrared, and microwave radiation. As opposed to visible and infrared techniques that must rely on information stemming from the tops of the clouds, microwave radiation penetrates clouds and rain and is independent of the sun as a source of illumination. This has given rise to a long list of passive microwave algorithms.[1–13] Passive microwave observations of Earth's atmosphere are of great importance in the detection and measurement of clouds and precipitation on a global scale. The retrieval scheme that

Received 24 December 2003; revision received 18 October 2004; accepted for publication 19 October 2004. Copyright © 2004 by the American Institute of Aeronautics and Astronautics, Inc. All rights reserved. Copies of this paper may be made for personal or internal use, on condition that the copier pay the $10.00 per-copy fee to the Copyright Clearance Center, Inc., 222 Rosewood Drive, Danvers, MA 01923; include the code 0887-8722/05 $10.00 in correspondence with the CCC.

*Research Scholar, Heat Transfer and Thermal Power Laboratory, Department of Mechanical Engineering.
†Scientist, Meteorology and Oceanography Group.
‡Associate Professor, Heat Transfer and Thermal Power Laboratory, Department of Mechanical Engineering; balaji@iitm.ac.in. Member AIAA.
§Professor, Heat Transfer and Thermal Power Laboratory, Department of Mechanical Engineering.

links the observed intensity and polarization to physical parameters (such as temperature, humidity, rain rate, path integrated water, or ice mass) is often set up as an optimization problem that utilizes forward calculations. Numerical models are used to compute the microwave radiation within a well-defined atmosphere. The inversion of such calculations gives the retrieval algorithm. In view of the preceding statements, it is clear that the quality of the retrieval algorithm is directly connected to 1) the accuracy of the physical model of the atmosphere, 2) the quality of the forward calculations, and 3) the intrinsic robustness and efficiency of the optimization procedure used for the retrieval.

The present work is concerned with obtaining the brightness temperature (the term used to represent intensity of radiation) emerging from the top of a multilayered, one-dimensional atmosphere in the microwave region. The physical processes involved are emission, absorption, scattering, and emission at the lower boundary. By the use of a known temperature profile and properties throughout the medium, a finite volume method is used to solve the governing time-independent radiative transfer equation, which represents radiation transfer through the participating medium, to obtain the brightness temperature corresponding to each microwave frequency. From a review of the literature, it is clear that using the finite volume method is new for the class of problems just presented. The finite volume method was first proposed by Briggs et al.[14] in the field of neutron transport. Raithby and Chui[15] gave a finite volume formulation for the first time for radiative heat transfer in a participating medium.

Physical Model

One-dimensional geometry, although simple, is a good approximation for many physical situations, such as heat transfer in insulation, the atmosphere, and large furnaces. It also serves as a building block for the analysis of other geometries. The one-dimensional geometry used for representing atmospheres in the present study is shown in Fig. 1. The bottom surface is considered to be a perfectly rough surface (Lambertian surface) with an emissivity of ε. The atmosphere is assumed to be made of up to n nongray, nonisothermal, vertically inhomogeneous layers, in which each layer is characterized by different absorption, emission, and scattering coefficients. At the top of the atmosphere, cosmic background radiation at 2.7 K is assumed.

The one-dimensional domain is divided into N_z control volumes of length Δz in the z direction. In Fig. 1, control volumes for a single layer are shown. The total spherical solid angle of 4π is subdivided into M discrete, nonoverlapping, solid angles of size ω^ℓ, $\ell = 1, 2, 3, \ldots, M$, where M represents the number of directions in the total polar angle γ of π radians. In this case, because of symmetry, the intensity is a function of z and γ only, that is, for a given (z, γ), the intensity is the same for all azimuthal angles ϕ from 0 to 2π.

General Formulation

The problem to be solved is the transfer of monochromatic radiation in a scattering, absorbing, and emitting plane-parallel slab with a Lambertian surface at the lower boundary. The solution to this problem will give us the intensity leaving the top of the atmosphere over the entire range of microwave frequencies. The formulation is based on a finite volume method proposed by Raithby and Chui.[15]

The change in intensity over the path length s for a participating medium through which radiative energy travels is found by summing the contributions from 1) absorption, 2) scattering away from the direction $\boldsymbol{s}$, 3) emission, and 4) scattering into the direction of $\boldsymbol{s}$. This can be written as[16]

$$\frac{\mathrm{d}I_\lambda}{\mathrm{d}s} = -(\kappa_\lambda + \sigma_{s\lambda})I_\lambda(s) + [\kappa_\lambda I_{b\lambda}(s) + \sigma_{s\lambda}\bar{I}_\lambda(s, \omega, \omega')] \tag{1}$$

In the microwave region, at typical tropospheric temperatures, the blackbody intensity can be approximated using a Rayleigh–Jeans formula (see Ref. 16) and is given by

$$I_{b\lambda} = [2C_1 T(z)] \Big/ C_2 \lambda^4 \tag{2}$$

Because the intensity is directly proportional to temperature, it is common to replace $I_{b\lambda}$ with $T(z)$ in the microwave region, which implies that the intensities must be interpreted as brightness temperatures. The in-scattering term is given by

$$\overline{I_\lambda}(s, \omega, \omega') = \frac{1}{4\pi}\int_{\omega'=0}^{4\pi} I_\lambda(s, \omega')\Phi(\lambda, \omega, \omega')\,\mathrm{d}\omega' \tag{3}$$

The anisotropic scattering property of the particles is approximated by retaining only a certain number of terms of the Legendre polynomial series expansion. A linear anisotropic scattering model is one in which only the first two terms of the series are used and that has the following mathematical representation for the phase function[13]:

$$\Phi(\lambda, \omega, \omega') = 1 + 3g(\lambda, z)[\cos\gamma'\cos\gamma + \sin\gamma'\sin\gamma\cos(\phi' - \phi)] \tag{4}$$

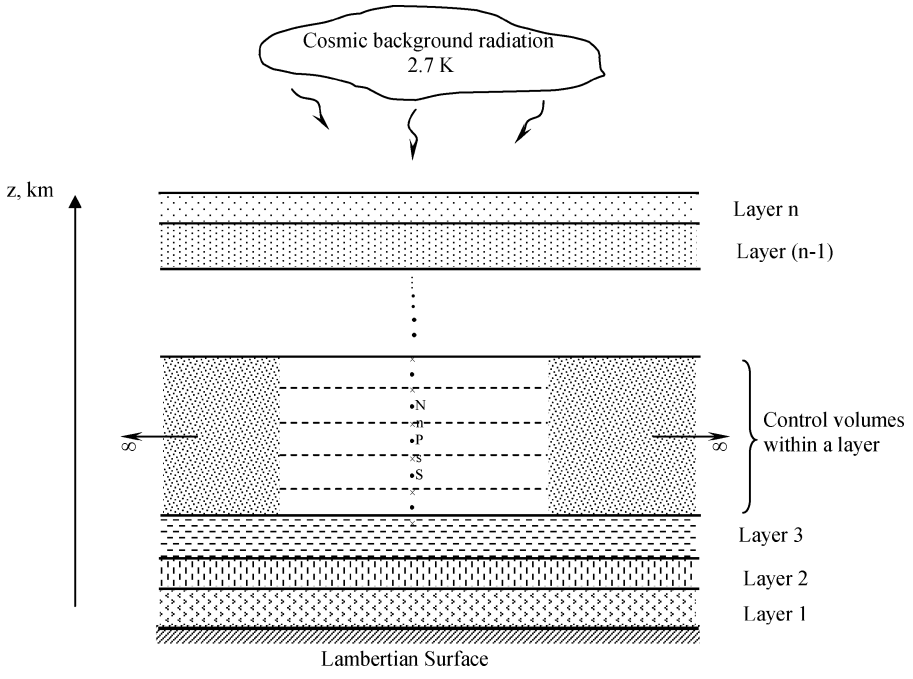

Fig. 1 Schematic of multilayered medium with control volumes.

Equation (1) is integrated over the control volume v_p and ω^ℓ. Approximating all of the variables on the right-hand side of Eq. (1) as constant at the nodal value while carrying out the volume integration, we get

$$\sum_{f=n,s} A_f \int_{\omega^l} I_{\lambda f}(\boldsymbol{s}\cdot\boldsymbol{n}_f)\,\mathrm{d}\omega$$

$$= \left[-(\kappa_{\lambda P}+\sigma_{s\lambda P})I^\ell_{\lambda P} + \kappa_{\lambda P} I^\ell_{b\lambda P} + \sigma_{s\lambda P}\bar{I}^\ell_{\lambda P}\right] v_P \omega^\ell \tag{5}$$

Here, $I_{\lambda f}$ is determined using a relationship between $I_{\lambda f}$ and the nodal point values $I_{\lambda N}$ and $I_{\lambda S}$. The value of $I_{\lambda f}$ is found by tracing back along the path taken by the ray in reaching f along the negative $\boldsymbol{s}$ direction until a location is reached at which the intensity can be obtained by interpolation between the nodal values. The schematic representation of backtracing is shown in Fig. 2. The interpolation point is designated uf. The unit vector $\boldsymbol{s}$ is written as

$$\boldsymbol{s} = \bar{\boldsymbol{i}}\sin\gamma\cos\phi + \bar{\boldsymbol{j}}\sin\gamma\sin\phi + \bar{\boldsymbol{k}}\cos\gamma \tag{6}$$

Equation (1) can now be written as

$$\frac{\mathrm{d}I_\lambda}{\mathrm{d}s} + \beta_\lambda I_\lambda = \beta_\lambda R_\lambda \tag{7}$$

where $\beta_\lambda = \kappa_\lambda + \sigma_{s\lambda}$ (called the extinction coefficient) and $R_\lambda = (\kappa_\lambda I_{b\lambda} + \sigma_{s\lambda}\overline{I_\lambda})/\beta_\lambda$. The term R_λ in the path from uf to f can be expressed using a Taylor series expansion of R_λ about f. With a two-term expansion, for example, Eq. (7) can be written as

$$\frac{\mathrm{d}I_\lambda}{\mathrm{d}s} + \beta_\lambda I_\lambda = \beta_\lambda\left[R_{\lambda f} - \left(\frac{\partial R_\lambda}{\partial s}\right)_f (S-s)\right] \tag{8}$$

Integration of Eq. (8) over a path length S from uf to f is performed to estimate the value of $I_{\lambda f}$ in terms of $I_{\lambda uf}$ as

$$I_{\lambda f} = I_{\lambda uf} e^{-\beta_{\lambda_f} S} + R_{\lambda f}(1 - e^{-\beta_{\lambda_f} S})$$

$$-\left[\left(\frac{\partial R_\lambda}{\partial s}\right)_f \Big/ \beta_{\lambda_f}\right]\left[1 - e^{-\beta_{\lambda_f} S}\left(1+\beta_{\lambda_f} S\right)\right] \tag{9}$$

Substitution of Eq. (9) into Eq. (5) results in the expression of nodal intensity $I^l_{\lambda P}$. Hence, the total number of equations to be solved to obtain the intensity at all nodes for all directions is $N_z \times M$. The method of solution is as given by Swaminathan et al.[17] The radiation transfer at the walls is modeled using the radiosity–irradiation formulation, and the properties at any layer interface are obtained using a harmonic mean of the properties of the adjacent layers. Calculation of the absorption coefficient, scattering coefficient, and asymmetry factor g of each layer from the properties of the atmosphere follows the procedure given by Kummerow.[13]

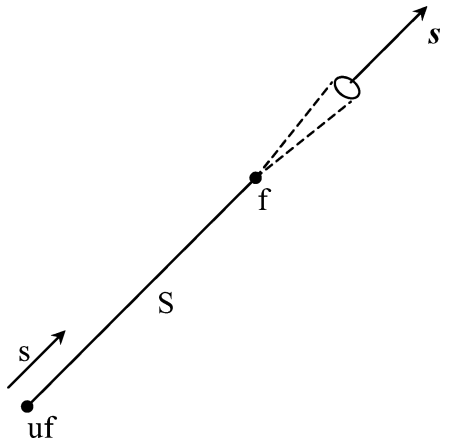

Fig. 2 Schematic of backtracing along $-s$ direction.

Validation

The code is validated by application to an example problem as follows. The radiation transfer between two parallel, diffuse, isothermal, infinitely long plates separated by an absorbing–emitting and linearly anisotropic scattering gray medium that is in radiative equilibrium is considered. The present computational results of dimensionless radiative heat flux $q^* = q/[\sigma(T^4_{\mathrm{bs}} - T^4_{\mathrm{us}})]$ for various values of optical thickness and different levels of anisotropic scattering are compared with the exact results given by Dayan and Tien.[18] From the values listed in Table 1, it is clear that the results obtained using the present procedure agree well with the exact solution, and the maximum modulus of error is 2.14%. This helps to validate the present model for a single layer.

Results and Discussion

The brightness temperature emerging at a viewing angle of 50 deg, obtained using a three-layer cloud model, is compared with the results obtained by Kummerow.[13] The bottom surface emissivity, temperature, and lapse rate are assumed to be 0.5, 300 K, and 5 deg/km, respectively. The relative humidity throughout the cloud is set constant at 80%. The nonprecipitating cloud liquid water (CLW) is also assumed constant with a value of 0.1 g/m^3. The hydrometeor profile is assumed to be 16 mm/h throughout the cloud. From the bottom surface to 5 km (first layer), the hydrometeors are assumed liquid. From 5 to 8 km (second layer), the hydrometeors are equally divided among liquid and frozen drops, and between 8 and 11 km (third layer) all of the hydrometeors are assumed frozen. The values of absorption coefficient, scattering coefficient, and asymmetry factor for these three layers, corresponding to the respective microwave frequencies, are listed in Table 2. A comparison of the brightness temperatures obtained in the present study with those of Kummerow,[13] corresponding to six different microwave frequencies, is shown in Table 3.

It is evident from Table 3 that the brightness temperature values, as calculated in this study, do not match well with those obtained using the Eddington approximation for some frequencies. To investigate this further, the following procedures were performed with a specific aim of removing any artifact introduced by the numerical procedure:

1) Use of different types of grids, namely, a) uniform grids with nodes placed at the interface and b) cosine grids for each layer.

2) Change the order of the scheme from first to second order.

3) Use three terms of Taylor expansion of R_λ, instead of a two-term expansion.

4) Approximate the phase function Φ using a) the first three terms of the Legendre polynomial series expansion, and b) the first four terms of the Legendre polynomial series expansion.

The preceding experiments failed to produce any significant change in the results, as can be seen in Table 4. The basic model in Table 4 corresponds to use of uniform grids with nodes not placed at the interface, a first-order scheme, and a two-term expansion for R_λ. Table 4 confirms that the numerical scheme employed in the

Table 1 Comparison of dimensionless heat flux q^* for different cases of anisotropic scattering

		$g=-0.3$		$g=0.0$		$g=0.3$	
κ, km^{-1}	σ_s, km^{-1}	q^* (present)	q^*(exact[18])	q^*(present)	q^*(exact[18])	q^*(present)	q^*(exact[18])
0.0222	0.0777	0.9010	0.9010	0.9154	0.9160	0.9303	0.9310
0.1111	0.3888	0.6630	0.6630	0.7038	0.7040	0.7500	0.7500
0.2222	0.7777	0.5143	0.5050	0.5530	0.5530	0.5982	0.6110
0.6666	2.3333	0.2602	0.2600	0.3010	0.3010	0.3582	0.3580
2.2222	7.7777	0.0968	——	0.1166	——	0.1466	——

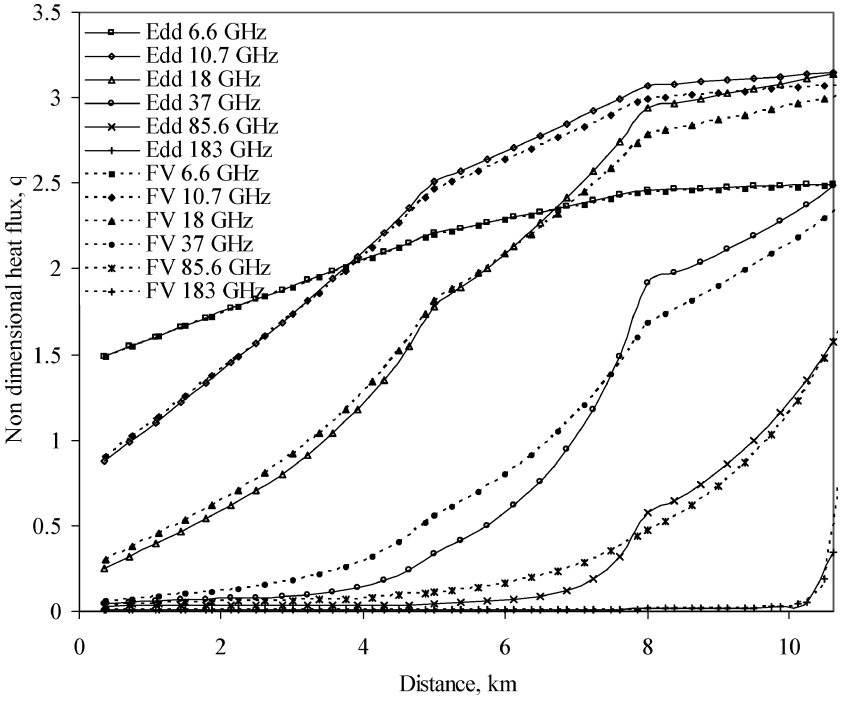

Fig. 3 Variation of dimensionless heat flux with distance from bottom surface.

Table 2 Properties of three-layer cloud model for various microwave frequencies[13]

Properties	Frequency, GHz					
	6.6	10.7	18.0	37.0	85.6	183.0
	0–5 km layer (hydrometeors assumed liquid)					
κ_λ, km^{-1}	0.02112	0.091238	0.267072	0.71253	1.47147	13.9216
$\sigma_{s\lambda}$, km^{-1}	0.00088	0.006762	0.053928	0.45747	1.25853	1.4784
g	0.091	−0.17	−0.082	0.010	0.276	0.539
	5–8 km layer (hydrometeors equally divided among liquid and frozen drops)					
κ_λ, km^{-1}	0.01172	0.035872	0.106875	0.380844	0.90372	7.0477
$\sigma_{s\lambda}$, km^{-1}	0.00028	0.002128	0.018125	0.215156	1.13628	2.4123
g	0.045	0.014	−0.010	0.091	0.394	0.522
	8–11 km layer (hydrometeors assumed frozen)					
κ_λ, km^{-1}	0.001872	0.004998	0.014191	0.045567	0.1218	3.1624
$\sigma_{s\lambda}$, km^{-1}	0.000128	0.001002	0.008809	0.137433	1.3282	2.7376
g	0.012	0.031	0.087	0.305	0.516	0.539

present study is reliable and accurate. It was also observed that the differences in the brightness temperature values between those of the present study and those by Kummerow[13] were within 0.5 K when only one uniform layer was considered. However, the agreement in the brightness temperature values was not good if the number of layers used was more than one. (See Table 3.) Note that, in the study by Kummerow,[13] differences between an eight-stream discrete ordinate solution and an analytical Eddington solution range up to 6 K when only one uniform layer of hydrometeors was considered. However, the differences never exceeded 3 K when realistic, multilayered cloud hydrometeor profiles were used. For multilayer models, one would expect the two approaches to disagree more because such a model with high scattering coefficients in one or more layers would put the simplistic Eddington approximation to a severe test. In our quest to determine the reasons for the disagreement in brightness temperatures, it is instructive to perform another exercise of looking at the variation of local dimensionless heat flux with distance for different frequencies. The variation for the three-layer model seen in Fig. 3 is indeed revealing in the sense that, as expected, at those frequencies where the brightness temperatures do not agree, there is also a considerable difference in the heat flux values between the Eddington results and the present results. In Fig. 3, "Edd" represents the Eddington solution and "FV" represents the finite volume solution. To further confirm that no discrepancies exist in the continuity of heat flux at the layer interface, the same three-layer model that was described in Table 3 was used between the two parallel plates under radiative equilibrium, problem (1), and it was found that the heat flux emerging out of the top and bottom plates turned out to be equal. Given this uniformity, it is clear that the likely cause now points to the scattering coefficient. This is systematically explored in the ensuing sections.

Table 3 Comparison of brightness temperatures calculated using the present finite volume method with those obtained using an analytical Eddington solution

Method	Frequency, GHz					
	6.6	10.7	18.0	37.0	85.6	183.0
Present finite volume method, brightness temperature, K	203.2	254.1	249.2	200.1	154.4	229.6
Analytical Eddington solution (Kummerow[13]), brightness temperature, K	203.4	259.9	261.9	216.9	158.3	228.9

Table 4 Comparison of brightness temperatures for various frequencies with the present finite volume method for different modifications of the basic model

Frequency, GHz	6.6	10.7	18.0	37.0	85.6	183.0
Nodes not at the interface of two layers						
Basic model	203.19	254.10	249.21	200.13	154.42	229.62
Uniform grid, second-order scheme, three-term expansion of R_λ	203.19	254.10	249.21	200.17	154.47	229.88
Uniform grid, second-order scheme, three-term expansion of R_λ, approximation of phase function using first three terms	203.18	254.01	249.15	200.17	154.50	229.63
Uniform grid, second-order scheme, three-term expansion of R_λ, approximation of phase function using first four terms	203.18	254.06	249.17	200.28	155.02	230.28
Cosine grid, second-order scheme, three-term expansion of R_λ	203.19	254.10	249.21	200.13	154.42	229.63
Nodes at the interface of two layers						
Uniform grid, second-order scheme, three-term expansion of R_λ	203.17	254.09	249.22	200.14	154.42	229.65

Table 5 Profiles of atmosphere at five different locations obtained from the freely available data sets of the ECMWF

Layer	Pressure, mbar	Temperature, K	Height, km	Humidity, %	CLW, g/m^3	Rain rate, mm/h	Ice content, mm/h
Location = 86133, wind speed = 11 m/s, sea surface temperature = 292.4 K							
1	1012.604	292.140	0.070	75.368	0.000	0.300	0.000
2	992.913	291.120	0.230	76.166	0.000	0.300	0.000
3	964.272	289.270	0.480	79.293	0.000	0.300	0.000
———	———	———	———	———	———	———	———
30	20.000	214.540	26.040	0.500	0.000	0.000	0.000
Location = 86134, wind speed = 8.3 m/s, sea surface temperature = 292.5 K							
1	1012.743	292.360	0.070	76.232	0.000	0.700	0.000
2	993.049	291.430	0.230	76.628	0.000	0.700	0.000
3	964.404	289.640	0.480	79.528	0.000	0.700	0.000
———	———	———	———	———	———	———	———
30	20.000	214.600	26.040	0.497	0.000	0.000	0.000
Location = 86135, wind speed = 12.3 m/s, sea surface temperature = 292.6 K							
1	1012.820	292.440	0.070	76.673	0.000	0.900	0.000
2	993.125	291.570	0.230	76.850	0.000	0.900	0.000
3	964.478	289.930	0.480	79.496	0.000	0.900	0.000
———	———	———	———	———	———	———	———
30	20.000	214.750	26.040	0.488	0.000	0.000	0.000
Location = 86136, wind speed = 12.0 m/s, sea surface temperature = 292.6 K							
1	1012.759	292.410	0.070	76.133	0.000	0.100	0.000
2	993.064	291.490	0.230	76.725	0.000	0.100	0.000
3	964.419	290.070	0.480	77.888	0.000	0.100	0.000
———	———	———	———	———	———	———	———
30	20.000	214.940	26.040	0.476	0.000	0.000	0.000
Location = 86138, wind speed = 8.3 m/s, sea surface temperature = 293 K							
1	1012.820	292.960	0.070	66.443	0.000	0.000	0.000
2	993.125	291.900	0.230	67.091	0.000	0.000	0.000
3	964.478	290.080	0.480	70.438	0.000	0.100	0.000
———	———	———	———	———	———	———	———
30	20.000	215.290	26.050	0.475	0.000	0.000	0.000

Test Cases

A grid independence study was carried out in a manner similar to that reported by Swaminathan et al.[17] The number of directions was fixed as 20, and the number of control volumes per layer was fixed as 10 when scattering constituents are present. There are two control volumes per layer when scattering constituents are not present.

Case 1

Some representative European Centre for Medium-Range Weather Forecasts (ECMWF) profiles of the atmosphere at five different typical locations above the sea surface were taken from Ref. 19 out of a globally covered database of $1.125^\circ \times 1.125^\circ$ spatial resolution for 1 August 1995. Gairola et al.[20] also used these global data for radiative transfer simulations for the development of an algorithm for the estimation of rainfall from the Tropical Rainfall Measuring Mission radar and radiometric observations. The data used here at five oceanic locations are shown in Table 5. The locations 86133–86138, specified in Table 5, correspond to some arbitrary locations on the sea surface. The comparison of brightness temperatures obtained using the Eddington approximation and those obtained with the present finite volume method for six different microwave frequencies, which are of interest in remote sensing for both horizontal as well as for vertical polarization, are shown in Table 6. The maximum difference in brightness temperature between these models turns out to be 11.3 K for the data given in Table 6.

For the case of no scattering, the columns containing rain rate and ice content are set to zero in Table 5. The comparison of brightness temperatures between the two models is shown in Table 7. The differences between these two models were within 2 K over the entire range of microwave frequencies considered here.

Case 2: Sensitivity Analysis

The profile at location 86135 is taken as the base, and perturbations were performed separately for humidity, CLW, rain rate, and ice content values in each layer, and the sensitivity of the brightness temperatures for different microwave frequencies is studied. The perturbations are carried out by multiplying the base values by some constants whose lower and upper bound varies between 0 and 30 in increasing order to obtain a different set of profiles, and, in the process, care is taken such that the following criteria are established: 1) Humidity content does not exceed 100% for any of the layers. 2) CLW content does not exceed 0.5 g/m^3 for any of the layers.

Table 6 Comparison of brightness temperatures comparison for realistic cloud models obtained from the ECMWF

		Brightness temperature, K, by location														
		86133			86134			86135			86136			86138		
Frequency, GHz	Polarization	Eddington	Present	Percent difference[a]	Eddington	Present	Percent difference[a]	Eddington	Present	Percent difference[a]	Eddington	Present	Percent difference[a]	Eddington	Present	Percent difference[a]
6.6	*H*	91.9	92.2	0.33	92.3	92.6	0.32	95.4	95.8	0.42	94.3	94.7	0.42	91.6	91.9	0.33
	V	158.1	158.3	0.13	159	159.2	0.13	160.1	160.4	0.19	159.5	159.7	0.13	158.7	158.9	0.13
10.7	*H*	103.8	104.4	0.57	106.9	107.7	0.74	112.3	113.3	0.88	108.7	109.4	0.64	104	104.7	0.67
	V	167.2	167.5	0.18	170	170.6	0.35	172.4	173.1	0.40	170.1	170.6	0.29	168.3	168.7	0.24
18	*H*	142.2	143.9	1.18	152.4	154.9	1.61	161.8	164.6	1.70	152.1	153.8	1.11	144.2	145.9	1.17
	V	194.5	195.6	0.56	201.7	203.4	0.84	206.4	208.4	0.96	200.4	201.5	0.55	196.7	197.7	0.51
37	*H*	202.9	207	1.98	222.7	230.5	3.38	233.6	242	3.47	217	219.2	1.00	206.2	208.4	1.06
	V	236.3	239.3	1.25	246.8	253	2.45	251.9	258.8	2.67	244.2	245.5	0.53	239.3	240.6	0.54
85.6	*H*	266.4	272.8	2.35	262.9	273.6	3.91	261.1	272.4	4.15	270.8	271.7	0.33	270.6	271.9	0.48
	V	270.2	276	2.10	263.8	274.3	3.83	261.5	272.6	4.07	273.1	273.8	0.26	274.5	275.4	0.33
183	*H*	227.6	227.2	0.18	227.2	227	0.09	227.1	226.9	0.09	227.3	226.8	0.22	227.2	226.8	0.18
	V	227.6	227.2	0.18	227.2	227	0.09	227.1	226.9	0.09	227.3	226.8	0.22	227.2	226.8	0.18

[a]Percent difference = (100 × |present-Eddington|)/present.

Table 7 Comparison of brightness temperatures without scattering by perturbing the data obtained from the ECMWF

		Brightness temperature, K, by location														
		86133			86134			86135			86136			86138		
Frequency, GHz	Polarization	Eddington	Present	Percent difference[a]	Eddington	Present	Percent difference[a]	Eddington	Present	Percent difference[a]	Eddington	Present	Percent difference[a]	Eddington	Present	Percent difference[a]
6.6	*H*	91.3	91.6	0.33	90.8	91.1	0.33	93.5	93.9	0.43	94.1	94.4	0.32	91.4	91.7	0.33
	V	157.7	157.8	0.06	158.0	158.2	0.13	158.9	159.1	0.13	159.3	159.5	0.13	158.6	158.8	0.13
10.7	*H*	102.0	102.5	0.49	102.3	102.9	0.58	106.5	107.1	0.56	108.0	108.7	0.64	103.6	104.2	0.58
	V	166.0	166.3	0.18	167.1	167.4	0.18	168.6	169.0	0.24	169.7	170.1	0.24	168.0	168.4	0.24
18	*H*	137.5	138.9	1.01	140.6	142.1	1.06	147.1	148.6	1.01	150.5	152.1	1.05	143.1	144.7	1.11
	V	191.6	192.4	0.42	194.3	195.3	0.51	197.2	198.2	0.50	199.4	200.4	0.50	196.0	197.0	0.51
37	*H*	190.8	192.7	0.99	198.3	200.2	0.95	207.5	209.3	0.86	213.5	215.3	0.84	203.5	205.4	0.93
	V	229.9	231.0	0.48	234.8	235.8	0.42	239.0	240.0	0.42	242.3	243.3	0.41	237.8	238.8	0.42
85.6	*H*	265.6	266.2	0.23	268.5	268.9	0.15	270.3	270.5	0.07	270.7	270.8	0.04	270.5	270.8	0.11
	V	273.8	273.9	0.04	274.5	274.4	0.04	274.4	274.2	0.07	273.8	273.6	0.07	275.3	275.2	0.04
183	*H*	227.7	227.3	0.18	227.6	227.2	0.18	227.5	227.0	0.22	227.3	226.9	0.18	227.3	226.8	0.22
	V	227.7	227.3	0.18	227.6	227.2	0.18	227.5	227.0	0.22	227.3	226.9	0.18	227.3	226.8	0.22

[a]Percent difference = (100 × |present-Eddington|)/present.

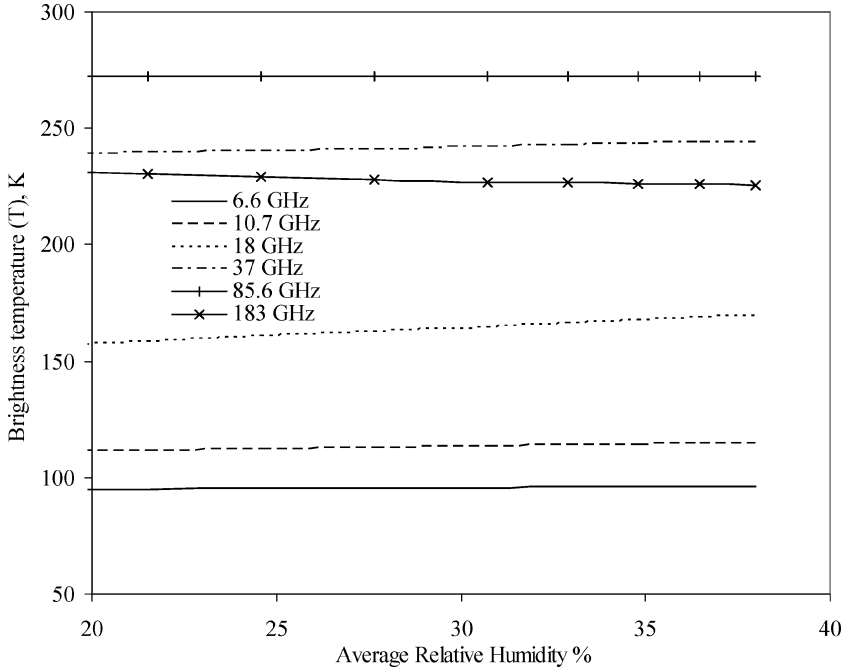

Fig. 4a Variation of brightness temperature with average humidity for the case of horizontal polarization and location 86135.

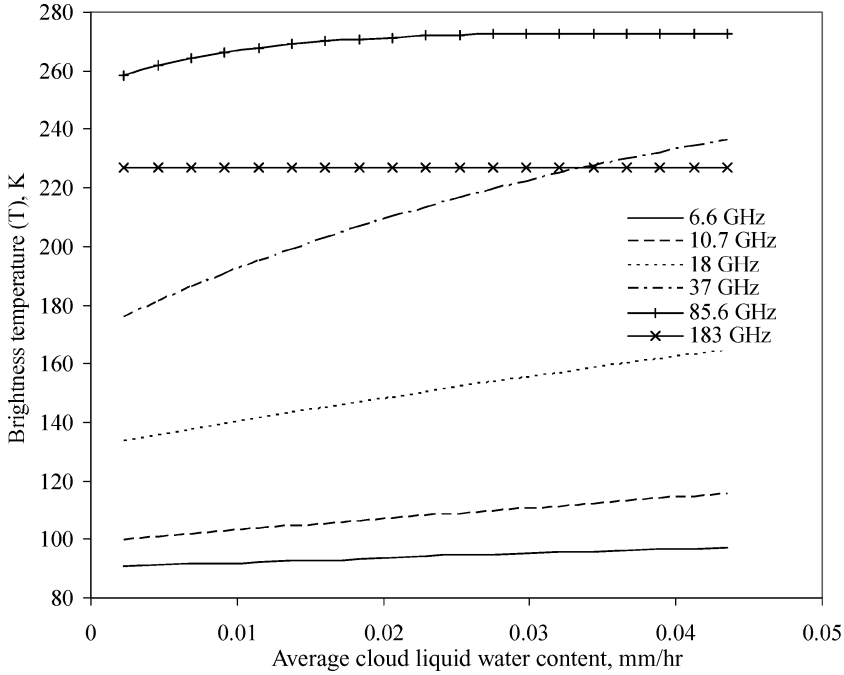

Fig. 4b Variation of brightness temperature with cumulative CLW content for the case of horizontal polarization and location 86135.

3) Both rain rate and ice content do not exceed 16.5 g/h for any of the layers. These criteria avoid unrealistic data generation. Figure 4a shows the variation of brightness temperature with average humidity content in the atmosphere. Here, the other properties are kept at base values, whereas the humidity content in each layer is perturbed by multiplying it by a constant (between 0.5 and 1.4) for all of the layers. Similarly, Figs. 4b–4d show the variation of brightness temperature with the average value of CLW, rain rate, and ice content, respectively. Figures 4 show the variation of brightness temperature for the case of horizontal polarization. The variation of brightness temperatures for vertical polarization follows similar trends. In light of this, it is evident that the brightness temperatures do not change significantly with an increase in the level of humidity content. The same is not the case for changes in other properties. Furthermore, for all of the cases, there is no significant variation in brightness temperature values corresponding to a frequency of 183 GHz. In summary, noticeable changes in brightness temperature values occur for 1) frequencies 18 and 37 GHz with increasing CLW content, 2) frequencies 6.6, 10.7, 18, and 37 GHz with increasing rainfall rate, and 3) frequencies 37 and 85.6 GHz with increasing ice content.

Also, whereas, in general, the brightness temperature values change with absorption and scattering coefficients, it is found that the difference in brightness temperature values between results of the present study and those obtained using the Eddington approximation increase sharply with an increase in the ratio of the scattering

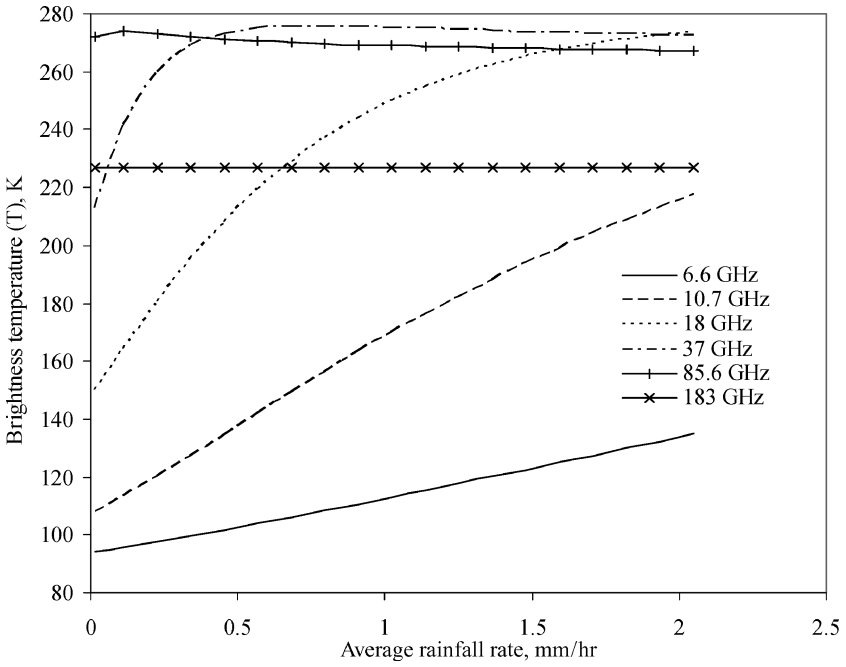

Fig. 4c Variation of brightness temperature with cumulative rainfall rate for the case of horizontal polarization and location 86135.

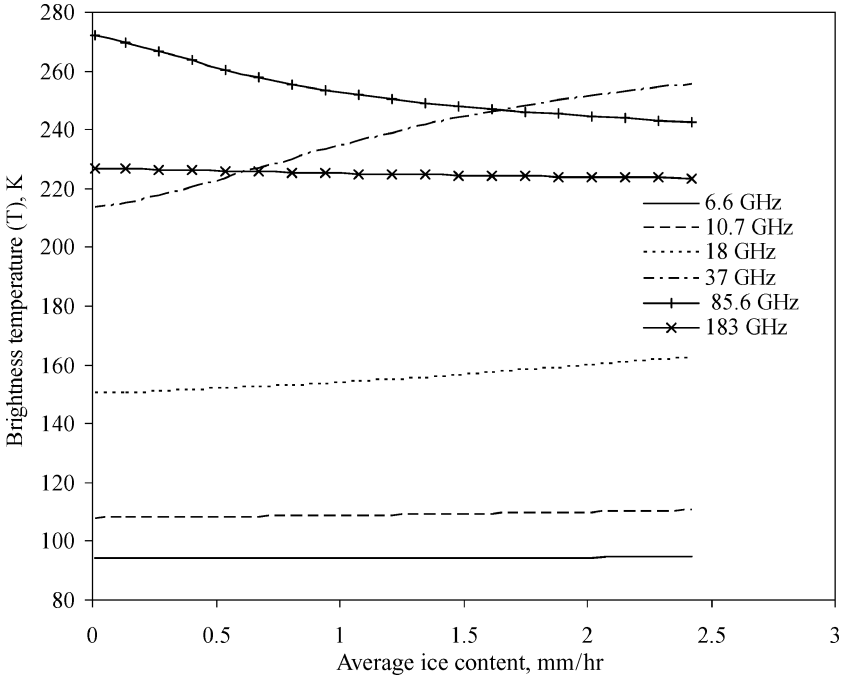

Fig. 4d Variation of brightness temperature with cumulative ice content for the case of horizontal polarization and location 86135.

to absorption coefficient. Figures 5a and 5b show the percentage deviation in brightness temperature between the two models with respect to the increase in the ratio of the average value of the scattering to absorption coefficient corresponding to an increase in rain rate and ice content, respectively. When the percentage deviation in brightness temperature between the two models was obtained, the brightness temperature value of the present model was used in the denominator. The curves in Figs. 5 are between the percentage deviations in brightness temperature with respect to the average value of the ratio of the scattering coefficient to the absorption coefficient because it was observed that the deviation between the two models is sensitive only to this ratio. Figures 5 clearly establish that the deviation in the brightness temperature value increases strongly and nonlinearly with an increase in the ratio of the scattering to the absorption coefficient. This shows that the analytical Eddington solution is not suitable for cases with large scattering to absorption coefficient values. In the present case, 20 directions were used to capture the scattering properties as opposed to the use of only two directions in the analytical Eddington model, and no approximation is involved in the representation of intensity as compared to that of the Eddington approximation. The present finite volume method is arguably better for the estimation of microwave radiation intensity in the range of parameters considered in this study. All of the preceding data confirm that the Eddington approximation is quite prone to error whenever scattering is dominant.

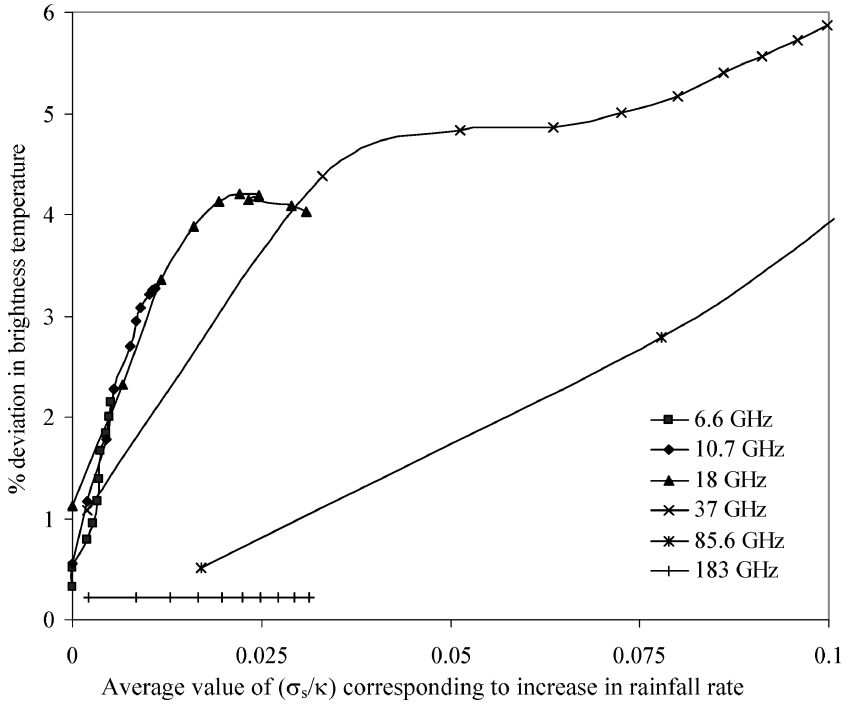

Fig. 5a Variation of percent deviation in brightness temperature values between Eddington approximation solution and finite volume solution.

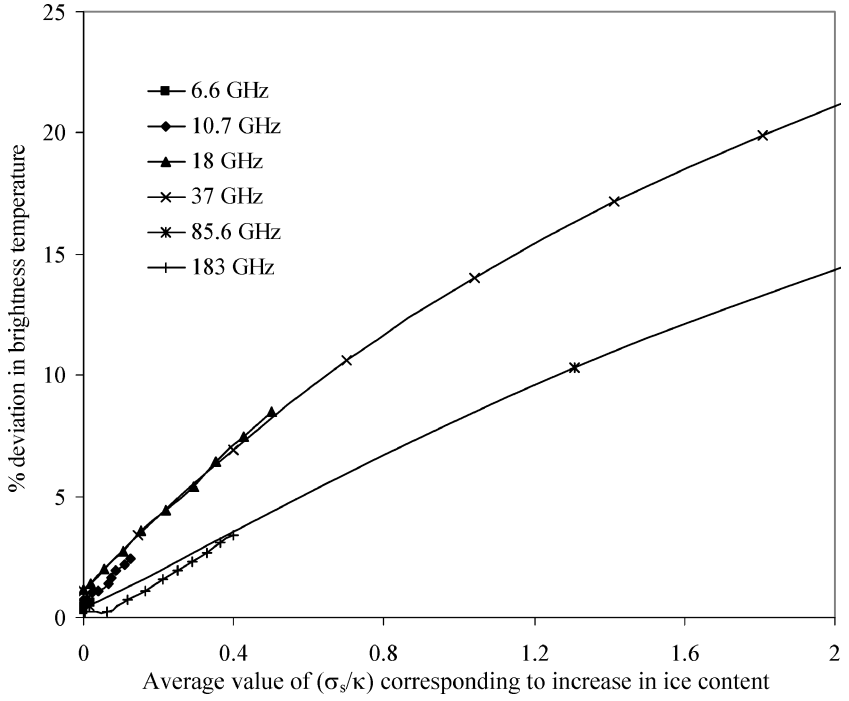

Fig. 5b Variation of percent deviation in brightness temperature values between Eddington approximation solution and finite volume solution.

Conclusions

A finite volume method for radiation has been used to determine the microwave radiation intensity leaving the top surface of a realistic atmospheric model. The results of the finite volume method have been demonstrated starting from a single-layer to a multilayer cloud model with and without scattering constituents and are compared with benchmark solutions and other approximate solutions. A sensitivity analysis has been carried out, and the variations of the microwave brightness temperature with respect to the change in the constituents of the atmosphere have been shown graphically. Note that with the increasing values of the ratio of the scattering to the absorption coefficients, the difference in the brightness temperatures calculated in the present study and in the analytical Eddington results increases dramatically. As a consequence of this, as well as that the model employed in the present study is more rigourous and realistic, the finite volume method presented in this study is demonstrably superior to the analytical Eddington model and is, hence, recommended for the estimation of intensity in the microwave region from multilayered cloud models.

Acknowledgments

The authors would like to express their gratitude to Christian D. Kummerow, Associate Professor, Department of Atmospheric Sciences, Colorado State University, for supplying the "analytical"

Eddington approximation model code used in this study and to the European Centre for Medium-Range Weather Forecasts for supplying realistic atmospheric profiles.

References

[1]Shettle, E. P., and Weinman, J. A., "The Transfer of Solar Irradiance Through Inhomogeneous Turbid Atmospheres Evaluated by Eddington's Approximation," *Journal of the Atmospheric Sciences*, Vol. 27, No. 7, 1970, pp. 1048–1055.

[2]Coakley, J. A., Jr., and Chylek, P., "The Two Stream Approximation in Radiative Transfer: Including the Angle of the Incident Radiation," *Journal of the Atmospheric Sciences*, Vol. 32, No. 2, 1975, pp. 409–418.

[3]Weinman, J. A., and Guetter, P. J., "Determination of Rainfall Distributions from Microwave Radiation Measured by the Nimbus-6 ESMR," *Journal of Applied Meteorology*, Vol. 16, No. 4, 1977, pp. 437–442.

[4]Wilheit, T. T., Chang, A. T. C., Rao, M. S. V., Rodgers, E. B., and Theon, J. S., "A Satellite Technique for Quantitatively Mapping Rainfall Rates Over the Oceans," *Journal of Applied Meteorology*, Vol. 16, No. 5, 1977, pp. 551–560.

[5]Weinman, J. A., and Davies, R., "Thermal Microwave Radiances from Horizontally Finite Clouds of Hydrometeors," *Journal of Geophysical Research*, Vol. 83, No. C6, 1978, pp. 3099–3107.

[6]Wilheit, T. T., Chang, A. T. C., King, J. L., Rodgers, E. B., Nieman, R. A., Krupp, B. M., Milman, A. S., Stratigos, J. S., and Siddalingaiah, H., "Microwave Radiometric Observations Near 19, 35, 37, 92, and 183 GHz of Precipitation in Tropical Storm Cora," *Journal of Applied Meteorology*, Vol. 21, No. 8, 1982, pp. 1137–1145.

[7]Wu, R., and Weinman, J. A., "Microwave Radiances from Precipitating Clouds Containing Aspherical Ice, Combined Phase and Liquid Hydrometeors," *Journal of Geophysical Research*, Vol. 89, No. D5, 1984, pp. 7170–7178.

[8]Kummerow, C., and Weinman, J. A., "Determining Microwave Brightness Temperatures from Precipitating Horizontally Finite and Vertically Structured Clouds," *Journal of Geophysical Research*, Vol. 93, No. D4, 1988, pp. 3720–3728.

[9]Mugnai, A., and Smith, E. A., "Radiative Transfer to Space Through a Precipitating Cloud at Multiple Microwave Frequencies, Part I: Model Description," *Journal of Applied Meteorology*, Vol. 27, No. 9, 1988, pp. 1055–1073.

[10]Smith, E. A., and Mugnai, A., "Radiative Transfer to Space Through a Precipitating Cloud at Multiple Microwave Frequencies, Part II: Results and Analysis," *Journal of Applied Meteorology*, Vol. 27, No. 9, 1988, pp. 1074–1092.

[11]Stamnes, K., Tsay, S. C., Wiscombe, W., and Jayaweera, K., "Numerically Stable Algorithm for Discrete-Ordinate-Method Radiative Transfer in Multiple Scattering and Emitting Layered Media," *Applied Optics*, Vol. 27, No. 12, 1988, pp. 2502–2509.

[12]Stephens, G. L., "Radiative Transfer Through Arbitrary Shaped Optical Media, I, A General Method of Solution," *Journal of the Atmospheric Sciences*, Vol. 45, No. 12, 1988, pp. 1818–1836.

[13]Kummerow, C., "On the Accuracy of the Eddington Approximation for Radiative Transfer in the Microwave Frequencies," *Journal of Geophysical Research*, Vol. 98, No. D2, 1993, pp. 2757–2765.

[14]Briggs, L. L., Miller, W. F., Jr., and Lewis, E. E., "Ray-Effect Mitigation in Discrete Ordinate-Like Angular Finite Element Approximations in Neutron Transport," *Nuclear Science and Engineering*, Vol. 57, No. 2, 1975, pp. 205–217.

[15]Raithby, G. D., and Chui, E. H., "A Finite-Volume Method for Predicting Radiant Heat Transfer in Enclosures with Participating Media," *Journal of Heat Transfer*, Vol. 112, No. 2, 1990, pp. 415–423.

[16]Siegel, R., and Howell, J. R., *Thermal Radiation Heat Transfer*, Taylor and Francis, Washington, DC, 1992, Chaps. 2 and 14.

[17]Swaminathan, V., Balaji, C., and Venkateshan, S. P., "Parameter Estimation in a Two-Layer Planar Gray Participating Medium," *Journal of Thermophysics and Heat Transfer*, Vol. 18, No. 2, 2004, pp. 187–192.

[18]Dayan, A., and Tien, C. L., "Heat Transfer in a Gray Planar Medium With Linear Anisotropic Scattering," *Journal of Heat Transfer*, Vol. 97, No. 1, 1975, pp. 391–396.

[19]Moreau, E., "Restitution de Paramètres Atmosphériques par Radiométrie Hyperfréquence Spatiale, Utilisation de Méthodes Neuronales," Ph.D. Dissertation, De l'Universite Paris 7, Paris, 2000.

[20]Gairola, R. M., Mallet, C., Viltard, N., and Moreau, E., "Estimation of Rainfall from TRMM-TMI and Precipitation Radar Using Neural Network Approach," CNES-ISRO, 2nd Scientific Workshop on Megha-Tropiques, Paris, July 2001.